

Blending Modified Gaussian Closure and Non-Gaussian Reduced Subspace Methods for Turbulent Dynamical Systems

Themistoklis P. Sapsis* and Andrew J. Majda
Courant Institute of Mathematical Sciences, New York University,
251 Mercer St., New York, 10012 NY

October 31, 2012

Abstract

Turbulent dynamical systems are characterized by persistent instabilities which are balanced by nonlinear dynamics that continuously transfer energy to the stable modes. To model this complex statistical equilibrium in the context of uncertainty quantification all dynamical components (unstable modes, nonlinear energy transfers, and stable modes) are equally crucial. Thus, order-reduction methods present important limitations. On the other hand UQ methods based on the tuning of the non-linear energy fluxes using steady state information (such as the modified quasilinear Gaussian (MQG) closure) may present discrepancies in extreme excitation scenarios. In this paper we derive a blended framework that links inexpensive second-order UQ schemes that model the full space (such as MQG) with high order statistical models in specific reduced-order subspaces. The coupling occurs in the energy transfer level by i) correcting the nonlinear energy fluxes in the full space using reduced subspace statistics, and ii) by modifying the reduced-order equations in the subspace using information from the full space model. The results are illustrated in two strongly unstable systems under extreme excitations. The blended method allows for the correct prediction of the second-order statistics in the full space and also the correct modeling of the higher-order statistics in reduced-order subspaces.

1 Introduction

The most fundamental property of turbulent dynamical systems, which distinguish them from all other problems of applied mathematics, is the presence of persistent instabilities over a large number of modes. From the dynamics point of view these instabilities are always balanced by a nonlinear energy transfer mechanism which acts both as a stabilizing factor for the unstable modes but also as a supplier of energy for the stable modes [16], leading to broad energy spectra. From the modeling or uncertainty quantification (UQ) point of view the presence of internal instabilities naturally leads to growth of any uncertainties present in the modeling equations, initial conditions, or parameters. Moreover, this synergistic activity of unstable modes, nonlinear energy transfer mechanisms, and

*Corresponding author: Email: sapsis@cims.nyu.edu, Tel.: +1 (516) 974-1545

stable modes, presents important modeling difficulties since all the above components are equally crucial for a correct description of the turbulent dynamics.

Therefore, by the very nature of turbulent dynamical systems it is hard to capture this elegant balance through a reduced-set of modes. Nevertheless there are a large number of applications where the dynamics ‘live’ in a low-dimensional space (e.g. flows with a laminar character having a very small number of instabilities) and for these systems it is efficient to perform order-reduction. Schemes based on this approach are essentially relying on the projection of the original system into a ‘suitable’ set of modes. These are chosen according to empirical criteria such as energy based proper orthogonal decomposition (POD) (see for example [17, 2]), linear-operator-theoretic model reduction methods, such as the balanced POD [3, 6], and more recently dynamically orthogonal (DO) field equations that follow from the original system equation [14, 13].

The effect of the projection on the linearized dynamics may not allow for the correct modeling of all the instabilities involved in the case where the modes are not sufficient in number or appropriately chosen. The same limitations hold for the modeling of intrinsically irreducible linearized dynamics (such as non-normal dynamics - see Section 4.1 in [15]) or even dynamical components, which despite the fact that they do not interact with other modes, their energy is important for the correct modeling (see Section 4.2.1 - case II in [15]). A blended approach based on the quasilinear Gaussian (QG) closure and DO equations was developed in [15] to resolve the misleading modeling of the linear dynamics due to the order-reduction. In this case a reduced-order DO approach was used just for the modeling of the nonlinear fluxes while the linear dynamics were modeled completely. The developed QG-DO method performed very well in systems with stable mean and important nonlinear energy fluxes where the system energy (or the attractors finite size) was caused mainly due to the external stochastic forcing.

It turns out however, that a reduced-order modeling approach even at the level of nonlinear energy fluxes is not sufficient to approximate adequately the synergistic activity of unstable, stable and nonlinear dynamics in a turbulent system. A first step towards this direction was the development of the modified quasilinear Gaussian closure (MQG) scheme [16]. Through a second-order statistical framework the collective effect of the non-Gaussian statistics or nonlinear dynamics is quantified in the energy transfer level using second-order steady-state information. Subsequently this nonlinear energy transfer mechanism is represented and coupled to the original linear dynamics. In contrast to other second-order schemes (e.g. mean square models [1, 9]) MQG not only recovers the correct steady state statistics but it does this by correctly modeling the energy flow between different dynamical components (or different locations of the spectrum). This leads to very good performance of the UQ scheme even in transient regimes where the energy and number of instabilities are much different than the statistical steady state used to diagnose the energy fluxes.

Despite its very good performance MQG is ‘tied’ to the steady-state statistics for which it is tuned. Therefore in extremely different excitation scenarios with spatially non-homogeneous or even localized action some discrepancies may occur. This is because, even though the MQG nonlinear energy fluxes are complete (full-order), they may not be able to model a specific dynamical scenario which is not present in the dynamics used to diagnose the nonlinear fluxes. Such a scenario can be, for example, injection of energy in high wavenumbers causing reverse flow of energy to large scale modes. In addition MQG can provide only second-order statistical information.

The goal of the present work is the improvement of the MQG scheme in extreme excitation scenarios that ‘push’ the system in very different dynamical regimes from those for which the MQG nonlinear fluxes have been tuned. To achieve this goal we will develop a blended framework of inexpensive, full-space, second-order UQ schemes (such as MQG) with high order statistical

models (such as the Fokker-Planck equation or Monte-Carlo simulation) in reduced-order subspaces (in the present work these will be DO subspaces). This is a particularly challenging task given the contradictory character of the two ingredient methods (MQG and DO). The coupling will be performed at the level of the energy fluxes by correcting the MQG fluxes using higher order-statistical information from a DO reduced order subspace for which the non-linear dynamics are modeled explicitly. On the other hand we will use the inexpensive second-order statistical model to maintain the correct energy content inside the DO subspace by modifying the reduced order equation so that it implicitly takes into account the interactions of the subspace dynamics with the dynamics lying outside of it. We will prove that this two-way coupling integrates naturally the two methods resulting in pure improvement relative to the MQG method.

The structure of the paper is as follows. In Section 2 we present and analyze the dynamics of two paradigm systems with persistently unstable dynamics: the unstable triad and the Lorenz 96 system. We illustrate how the nonlinear energy fluxes are connected with non-Gaussian statistics and based on this connection we explain why order-reduction techniques will not be able to describe the correct dynamics (see [15] for more discussion). In Section 3 we illustrate the limitations of blended methods that perform reduction at the level of energy fluxes such as QG-DO method. In Section 4 we present the MQG-DO method and we show how the coupling approach results in a natural blending of the two methodologies that leads to monotonic improvement with respect to the number of modes for which the full statistics are resolved. Finally, in Section 5 we illustrate the advantages of the new blended approach in a variety of time-dependent and time-independent examples exhibiting a strongly unstable character.

2 Dynamical systems with unstable mean

We will focus on the development of blended UQ techniques in order to describe the stochastic attractor of systems with persistently unstable mean. These are systems whose linearized dynamics are associated with an important number of positive Lyapunov exponents and therefore the careful and precise consideration of the nonlinear terms is crucial in order to avoid blowup or severe underestimation of energy in the UQ scheme [16].

This is a particularly challenging task given that our analysis will rely on the blending of two methodologies with completely opposing natures: one relying on the expensive statistical modeling of the dynamics in a low-dimensional subspace, and the other on the second-order (i.e. inexpensive) statistical modeling of the dynamics in the full space.

The generic system formulation on which our analysis and illustrations will be based is given by the quadratic system

$$\frac{d\mathbf{u}}{dt} = [L + D]\mathbf{u} + B(\mathbf{u}, \mathbf{u}) + \mathbf{F}(t) + \dot{W}_k(t; \omega) \sigma_k(t) \quad (1)$$

acting on $\mathbf{u} \in \mathbb{R}^N$. In the above equation and for what follows repeated indices will indicate summation. In some cases the limits of summation will be given explicitly to emphasize the range of the index.

In the above equation we have:

- L being a skew-symmetric linear operator representing the β -effect of Earth's curvature, topology etc. and satisfying,

$$L^* = -L.$$

- D being a negative definite symmetric operator,

$$D^* = D,$$

representing dissipative processes such as surface drag, radiative damping, viscosity, etc.

The quadratic operator $B(\mathbf{u}, \mathbf{u})$ conserves the energy by itself so that it satisfies

$$B(\mathbf{u}, \mathbf{u}) \cdot \mathbf{u} = 0.$$

Finally, $\mathbf{F}(t) + \dot{W}_k(t; \omega) \sigma_k(t)$ represents the effect of external forcing, which we will assume that it can be split into a mean component $\mathbf{F}(t)$ and a stochastic component with white noise characteristics. In what follows we give the basic setup for the exact statistical formulas which will be used in this paper.

We use a finite-dimensional representation of the stochastic field consisting of a fixed-in-time, N -dimensional, orthonormal basis

$$\mathbf{u}(t) = \bar{\mathbf{u}}(t) + Z_i(t; \omega) \mathbf{v}_i.$$

where $\bar{\mathbf{u}}(t) = \langle \mathbf{u}(t) \rangle$ represents the ensemble average of the response, i.e. the mean field, and $Z_i(t; \omega)$ are stochastic processes.

The mean field equation is given by

$$\frac{d\bar{\mathbf{u}}}{dt} = [L + D] \bar{\mathbf{u}} + B(\bar{\mathbf{u}}, \bar{\mathbf{u}}) + R_{ij} B(\mathbf{v}_i, \mathbf{v}_j) + \mathbf{F}. \quad (2)$$

Moreover the random component of the solution, $\mathbf{u}' = Z_i(t; \omega) \mathbf{v}_i$ satisfies

$$\frac{d\mathbf{u}'}{dt} = [L + D] \mathbf{u}' + B(\bar{\mathbf{u}}, \mathbf{u}') + B(\mathbf{u}', \bar{\mathbf{u}}) + B(\mathbf{u}', \mathbf{u}') + \dot{W}_k(t; \omega) \sigma_k(t) \quad (3)$$

By projecting the above equation to each basis element \mathbf{v}_i we obtain

$$\frac{dZ_i}{dt} = Z_j ([L + D] \mathbf{v}_j + B(\bar{\mathbf{u}}, \mathbf{v}_j) + B(\mathbf{v}_j, \bar{\mathbf{u}})) \cdot \mathbf{v}_i + B(\mathbf{u}', \mathbf{u}') \cdot \mathbf{v}_i + \dot{W}_k \sigma_k \cdot \mathbf{v}_i$$

From the last equation we directly obtain the evolution of the covariance matrix $R = \langle \mathbf{Z} \mathbf{Z}^* \rangle$

$$\frac{dR}{dt} = L_v R + R L_v^* + Q_F + Q_\sigma, \quad (4)$$

where we have:

i) the linear dynamics operator expressing energy transfers between the mean field and the stochastic modes (effect due to B), as well as energy dissipation (effect due to D) and non-normal dynamics (effect due to L)

$$\{L_v\}_{ij} = ([L + D] \mathbf{v}_j + B(\bar{\mathbf{u}}, \mathbf{v}_j) + B(\mathbf{v}_j, \bar{\mathbf{u}})) \cdot \mathbf{v}_i \quad (5)$$

ii) the positive definite operator expressing energy transfer due to the external stochastic forcing

$$\{Q_\sigma\}_{ij} = (\mathbf{v}_i \cdot \sigma_k) (\sigma_k \cdot \mathbf{v}_j). \quad (6)$$

iii) as well as the energy flux between different modes due to non-Gaussian statistics (or nonlinear terms) modeled through third-order moments

$$Q_F = \overline{Z_m Z_n Z_j} B(\mathbf{v}_m, \mathbf{v}_n) \cdot \mathbf{v}_i + \overline{Z_m Z_n Z_i} B(\mathbf{v}_m, \mathbf{v}_n) \cdot \mathbf{v}_j \quad (7)$$

The last term involves higher-order statistics and therefore suitable closure assumptions need to be made in order to setup a UQ scheme. *The modeling of the nonlinear energy fluxes Q_F based on a blended MQG and DO approach will be the main focus of this work.*

We note that the energy conservation property of the quadratic operator B is inherited by the matrix Q_F since

$$Tr[Q_F] = 2\overline{Z_m Z_n Z_i} B(\mathbf{v}_m, \mathbf{v}_n) \cdot \mathbf{v}_i = 2B(\mathbf{u}', \mathbf{u}') \cdot \mathbf{u}' = 0 \quad (8)$$

The above exact statistical equations will be the starting point for the approximation schemes that we will present and develop below. To illustrate and validate the developed UQ scheme we will consider two specific systems that belong to the general formulation (1) and mimic various mechanisms of turbulent dynamics. These will be the triad system in an unstable configuration, and the Lorenz-96 system under extreme time-space dependent excitation. In what follows we will give a detailed description of those examples as well as an analysis of the statistics and the associated energy transfers.

2.1 Unstable triad system

The first example that we consider is a simple but nevertheless instructive model, namely the triad system. This is a three-dimensional system with a quadratic part that is both divergence free and energy preserving. In the standard formulation the linear part consists of a dissipative operator that is negative-definite and a skew-symmetric operator. The nonlinear coupling in triad systems is generic of nonlinear coupling between any three modes in larger systems with quadratic nonlinearities [10, 11, 12]. We can think of this ‘toy’ problem as a ‘poormans’ approach to a full fluid system where the nonlinear terms, dissipation, and skew-symmetric part represent respectively the advection terms, the viscous dissipation, and the Coriolis effect while the stochastic noise represents the nonlinear interactions with other modes in a crude fashion.

In this standard formulation the mean is stable and the finite size of the stochastic attractor is by the external stochastic forcing. In this context the performance of the blended reduced-subspace algorithm based on the quasilinear Gaussian closure combined with dynamically orthogonal subspace reduction (QG-DO UQ scheme) has been proven to be very satisfactory [15]. However, in a turbulent system a fundamental factor is the internal system instabilities that make the mean unstable over various directions in phase space as is typical for anisotropic fully turbulent systems.

To examine this case we will modify the standard triad system configuration by imposing negative damping to one of the degrees of freedom creating a strong, persistent instability that makes the role of the external stochastic excitation to be of secondary importance. In particular the system that we consider is a three-dimensional special case of the generic quadratic system (1) given by

$$du_1 = (-\gamma_1 u_1 + \lambda_{12} u_2 + \lambda_{13} u_3 + \beta_1 u_3 u_2 + F_1) dt + \sigma_1 dW_1 \quad (9a)$$

$$du_2 = (-\gamma_2 u_2 - \lambda_{12} u_1 + \lambda_{23} u_3 + \beta_2 u_1 u_3 + F_2) dt + \sigma_2 dW_2 \quad (9b)$$

$$du_3 = (-\gamma_3 u_3 - \lambda_{13} u_1 - \lambda_{23} u_2 + \beta_3 u_2 u_1 + F_3) dt + \sigma_3 dW_3 \quad (9c)$$

with $\beta_1 + \beta_2 + \beta_3 = 0$. To obtain an unstable configuration in the steady state we choose negative damping for u_1 (the unstable mode) and positive for u_2 and u_3 : $\gamma_1 = -0.4$, $\gamma_2 = \gamma_3 = 2$. We choose

strong nonlinear coupling $\beta_1 = 2$, $\beta_2 = \beta_3 = -1$, and weak external noise $\sigma_1 = 0.25$, $\sigma_2 = \sigma_3 = 0.79$ since the energy of the system comes primarily from the instability of the first mode. The nonlinear coefficients are chosen to rapidly transfer energy from u_1 to u_2, u_3 with β_1 having the opposite sign of β_2, β_3 [10, 11, 12]. We also choose constant external forcing for the second and third degree of freedom, $F_2 = -1$, $F_3 = 1$, to achieve non-zero steady state values for u_2 and u_3 . This is essential for these modes to be active causing energy to flow towards them from u_1 so that the system will achieve a finite-energy steady state and u_1 will not blow up. The linear instability is always dominant for u_1 so we set $F_1 = 0$. Finally, we also add a skew symmetric component $\lambda_{12} = 0.03$, $\lambda_{13} = 0.06$, $\lambda_{23} = -0.09$.

The statistical equilibrium of this system relies exclusively on the strong energy transfer (due to nonlinear mechanisms) from the unstable modes to the stable ones. In Figure 1 (subplots a and d) we present the time series for the mean and variance for the three degrees of freedom showing clearly that u_1 is the dominant one. The time series for the third-order central moments responsible for nonlinear energy transfer

$$M_{ijk} = \langle (u_i - \bar{u}_i) (u_j - \bar{u}_j) (u_k - \bar{u}_k) \rangle,$$

where $\langle \cdot \rangle$ denotes averaging over the probability measure, are presented in subplot b for the first mode. These plots clearly indicate that there is a continuous energy transfer from the first mode that balances its unstable character. The latter is expressed through the eigenvalues of the linearized dynamics operator L_v given by (5) and shown in subplot c. The strong third-order moments (causing the strong nonlinear energy transfers) are in full agreement with the deformed shape of the stochastic attractor illustrated in subplots e (through a low-value contour of the probability density function that contains most of the probability) and f (through two-dimensional scatter diagrams).

Despite its low dimensionality the unstable triad example is a challenging case to validate and assess the performance of a blended UQ algorithm since the equilibrium relies on a very sensitive balance of nonlinear energy transfers (or equivalently third-order moments) and unstable dynamics. This connection has to be modeled very carefully in the UQ scheme in order to obtain meaningful results.

2.2 Lorenz 96 system

The second system that we study is the Lorenz 96 system (L-96) which is the simplest paradigm of a complex turbulent dynamical systems possessing properties found in realistic turbulent systems such as a linearly unstable mean state, important energy spanning the whole spectrum, a large number of persistent instabilities, and strong nonlinear energy transfers between modes. It is widely used as a test model for algorithms for prediction, filtering, and low frequency climate response [4, 5, 7, 9, 8]. Therefore, L-96 is a perfect candidate both to illustrate the limitations of existing UQ schemes but also to validate the derived UQ model [16].

The L-96 model is a discrete periodic system described by the equations

$$\frac{du_i}{dt} = u_{i-1} (u_{i+1} - u_{i-2}) - u_i + F_i, \quad i = 0, \dots, J-1 \quad (10)$$

with $J = 40$ and with F_i the deterministic forcing. We can easily observe that the energy conservation property for the quadratic part is satisfied (i.e. $B(\mathbf{u}, \mathbf{u}) \cdot \mathbf{u} = \mathbf{0}$) and the negative definite part has the diagonal form $D = -\mathbf{I}$.

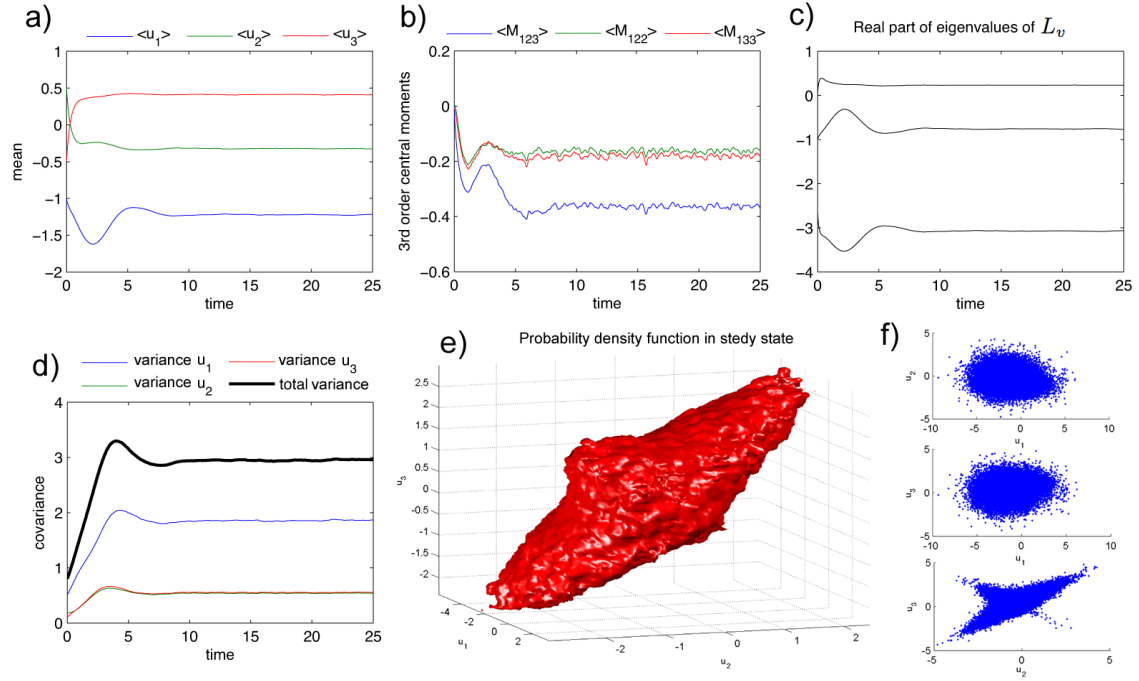


Figure 1: Triad system with one unstable direction: a) time series for the mean of \mathbf{u} ; b) time-series for the third-order central moments of \mathbf{u} involving the unstable mode; c) real part of the linearized dynamics $L_v(\bar{\mathbf{u}})$ eigenvalues; d) time series for the variance of the three DOF and the trace of the covariance matrix; e) a low-probability contour of the full pdf ($\{\mathbf{u} | f_{\mathbf{u}}(\mathbf{u}) = 10^{-6}\}$) in steady-state. This surface bounds the major part of the probability measure; f) 2D scatter plots in steady-state.

The model is designed to mimic baroclinic turbulence in the midlatitude atmosphere with the effects of energy conserving nonlinear advection and dissipation represented by the first two terms in (10). For sufficiently strong forcing values such as $F = 6, 8$ or 16 the L-96 is a prototype turbulent dynamical system which exhibits features of weakly chaotic dynamics ($F_i = 6$), strong chaotic dynamics ($F_i = 8$), and turbulent dynamics ($F_i = 16$) (cf. Figure 2 - first row).

In the L-96 system the external noise is zero, and therefore we have no such contribution in eq. (4), i.e. $Q_\sigma = 0$. Thus, uncertainty can only build-up from the unstable modes of the linearized dynamics - described by $L_v(\bar{\mathbf{u}})$. Moreover, by observing the statistical steady state spectrum of the response (Fig. 2 - second row) we notice that energy spans all the wavenumbers, both stable and unstable; a clear indication that energy is continuously transferred through the nonlinear fluxes Q_F caused by important third-order moments.

To obtain a more intuitive picture of the energy transfers between different dynamical components we project the statistical steady state solution to the empirical orthogonal function (EOF or POD) basis consisting of Fourier modes in the translation invariant system [7]. In particular let \mathbf{u}_∞ denote the statistical steady state solution in physical space for the L-96. We choose as a base \mathbf{v}_i the EOF modes that satisfy

$$\mathbf{C}_{uu}\mathbf{v}_j = \sigma_j^2\mathbf{v}_j, \quad j = 1, \dots, J$$

where, $\mathbf{C}_{uu} = \langle (\mathbf{u}_\infty - \bar{\mathbf{u}}_\infty)(\mathbf{u}_\infty - \bar{\mathbf{u}}_\infty)^* \rangle$ is the covariance matrix in physical space. We arrange the EOF modes, in descending order with respect to their energy, i.e. $\sigma_1^2 \geq \sigma_2^2 \geq \dots \geq \sigma_J^2$ and we represent the steady state solution as

$$\mathbf{u}_\infty = \bar{\mathbf{u}}_\infty + Z_{\infty i}(\omega)\mathbf{v}_i.$$

After projecting the statistical steady state solution to the EOF base we consider the third order statistics

$$M_{ijk} = \langle Z_{\infty i}Z_{\infty j}Z_{\infty k} \rangle.$$

This 3-tensor provides information about the energy exchanges between different dynamical components (that represent different energy part of the spectrum) occurring in the form of triad interactions. In Figure 2 - third row we present contours that include moments which are, in magnitude, 15% or larger than the maximum M_{ijk} . In other words for each forcing value we present the contour $|M_{ijk}| = 0.15 \max_{ijk} M_{ijk}$. The coloring is according to the value of the contained moments i.e. red for negative moments and blue for positive moments.

Even for the smallest value of F from those that we consider, we can clearly observe that the dominant nonlinear interactions occur in the form of triad energy exchanges involving very high energy modes and very low energy modes. This property reveals the challenge behind the precise modeling of the nonlinear fluxes Q_F since any attempt to ignore very low-energy dynamical components will have a dramatic impact on the energy transfer properties. This property is more pronounced as we go to more intense forcing.

The above property is also confirmed if we consider directly the nonlinear energy fluxes computed using only a few high-energy modes. In particular we saw that the nonlinear energy fluxes are given in terms of the third-order moments through equation (7). The partially modeled nonlinear energy fluxes (based only on the first $s \leq J$ modes) will be given by

$$Q_{F,s} = \sum_{n=1}^s \sum_{m=1}^s (M_{mnj}B(\mathbf{v}_m, \mathbf{v}_n) \cdot \mathbf{v}_i + M_{mni}B(\mathbf{v}_m, \mathbf{v}_n) \cdot \mathbf{v}_j) \quad (11)$$

In Figure 2 - fourth row we present what percentage of the nonlinear energy transfer terms is captured when we consider the s -most energetic modes. In particular for each s we present the ratio $q(s) = \frac{\max_{i,j} Q_{F,s}}{\max_{i,j} Q_F}$ (blue solid curve) together with the normalized energy of the modes (red dashed curve) and their cumulative energy (red solid curve). We observe that retaining the 14 most energetic modes (corresponding to more than 50% of the system energy) will not allow capturing more than 1-2% of the total nonlinear energy fluxes. Even, if we consider more modes this percentage increases very slowly.

Our recent MQG scheme [16] is able to alleviate this problematic behavior by directly modeling the fluxes Q_F in the second order level using a given statistical steady state (over which it is tuned). However, *the scope of the present work is to model the strong variations of the nonlinear energy fluxes (using third order statistics) caused by strong modifications of the conditions under which the MQG scheme has been tuned, i.e. to develop a UQ scheme that will be able to perform satisfactory in extreme conditions very far away from the tuned MQG spectrum.*

3 Limitations of existing UQ methodologies for turbulent systems

In this section we will provide an overview of existing UQ algorithms emphasizing their advantages and limitations for turbulent systems. In particular we will study the performance of UQ methods in turbulent systems with strong energy variations (over time) based i) on the reduced-order modeling of the nonlinear fluxes Q_F using dynamical orthogonality subspaces (QG-DO method [15]), and ii) on the modified quasilinear Gaussian (MQG) closure method [16] tuned over a specific energy level (i.e. a specific statistical steady-state).

3.1 Reduced order modeling of the dynamics of the nonlinear fluxes (QG-DO method)

Order-reduction techniques for UQ are based on the assumption that the modes that carry small amounts of energy do not have important influence on the global dynamics of the stochastic system. Based on this assumption order-reduction may be performed either on the complete dynamics (e.g. DO or POD equations) or just on the computation of the nonlinear fluxes Q_F (QG-DO method). The advantages of the latter method over standard reduction techniques have analyzed in detail in [15] and they are primarily related with the adequate modeling of i) non-normal dynamics which otherwise may be ignored, and ii) linear processes that contribute to the state covariance that plays an important role to the computation of the mean (eq. (2)).

Although in some systems this may indeed be the case, there are situations where this assumption does not hold, such as the systems presented in the previous section, where many low-energy modes act as nonlinear channels of energy that either transfer or dissipate important amounts of energy and therefore their effect has to be considered in the UQ scheme. Here we illustrate these limitations by applying the QG-DO methodology to the unstable triad and the L-96 system.

We proceed by recalling the QG-DO UQ scheme (see [15] for details). As mentioned previously, it is based on the reduced-order modeling of the nonlinear fluxes using statistical information from a low-dimensional subspace (called the DO subspace). The solution inside this s -dimensional

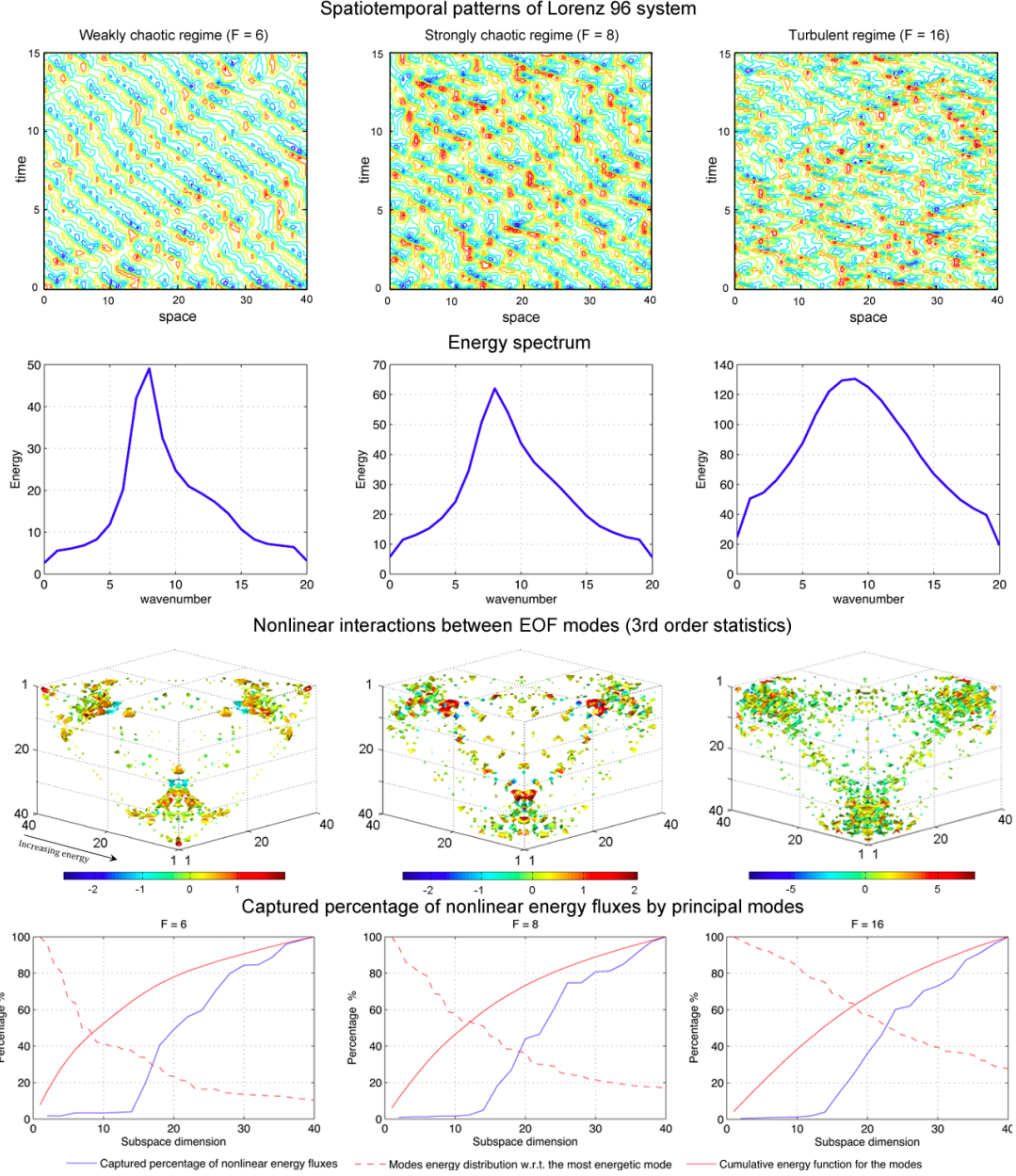


Figure 2: The three different dynamical regimes for the Lorenz-96 system. Spatiotemporal patterns (first row); Steady-state spectrum (second row); Third order central moments between principal modes. Only the significant moments are plotted (i.e. larger than 15% of the maximum) and are colored according to their magnitude and sign (third row); Captured percentage of the total nonlinear fluxes Q_F using the s most energetic modes (blue solid curve), captured percentage of energy using s modes (red solid curve), and the normalized energy of each mode with respect to the maximum energy (red dashed curve).

subspace is represented as

$$\mathbf{u}(t) = \bar{\mathbf{u}}(t) + \sum_{i=1}^s Y_i(t; \omega) \mathbf{e}_i(t)$$

where $\mathbf{e}_i(t)$, $i = 1, \dots, s$ are time-dependent modes and $s \ll N$ is the reduction order. The modes and the stochastic coefficients evolve according to the DO condition [14]. In particular the equations for the QG-DO scheme are as follows.

- *Equation for the mean*

The equation for the mean is obtained by averaging the original system equation (i.e. eq. (2))

$$\frac{d\bar{\mathbf{u}}}{dt} = [L + D] \bar{\mathbf{u}} + B(\bar{\mathbf{u}}, \bar{\mathbf{u}}) + R_{ij} B(\mathbf{v}_i, \mathbf{v}_j) + \mathbf{F}. \quad (12)$$

- *Equation for the stochastic coefficients and the modes*

Both the stochastic coefficients and the modes evolve according to the DO equations. The coefficients equations are obtained by a direct Galerkin projection and the DO condition

$$\begin{aligned} \frac{dY_i}{dt} &= Y_m ([L + D] \mathbf{e}_m + B(\bar{\mathbf{u}}, \mathbf{e}_m) + B(\mathbf{e}_m, \bar{\mathbf{u}})) \cdot \mathbf{e}_i \\ &+ (Y_m Y_n - C_{mn}) B(\mathbf{e}_m, \mathbf{e}_n) \cdot \mathbf{e}_i + \dot{W}_k \sigma_k \cdot \mathbf{e}_i \end{aligned} \quad (13)$$

Moreover, the modes evolve according to the equation obtained by stochastic projection of the original equation to the DO coefficients

$$\begin{aligned} \frac{\partial \mathbf{e}_i}{\partial t} &= [L + D] \mathbf{e}_i + B(\bar{\mathbf{u}}, \mathbf{e}_i) + B(\mathbf{e}_i, \bar{\mathbf{u}}) + B(\mathbf{e}_m, \mathbf{e}_n) \langle Y_k Y_m Y_n \rangle C_{ik}^{-1} \\ &- \mathbf{e}_j ([L + D] \mathbf{e}_i + B(\bar{\mathbf{u}}, \mathbf{e}_i) + B(\mathbf{e}_i, \bar{\mathbf{u}}) + B(\mathbf{e}_m, \mathbf{e}_n) \langle Y_k Y_m Y_n \rangle C_{ik}^{-1}) \cdot \mathbf{e}_j \end{aligned} \quad (14)$$

- *Equation for the covariance*

The equation for the covariance will be the exact equation (4) with approximated nonlinear fluxes

$$\frac{dR}{dt} = L_v R + R L_v^* + Q_{F,s} + Q_\sigma$$

where the *nonlinear fluxes are computed using reduced-order information from the DO subspace*

$$Q_{F,s} = \langle Y_m Y_n Y_k \rangle (B(\mathbf{e}_m, \mathbf{e}_n) \cdot \mathbf{v}_i) (\mathbf{v}_j \cdot \mathbf{e}_k) + \langle Y_m Y_n Y_k \rangle (B(\mathbf{e}_m, \mathbf{e}_n) \cdot \mathbf{v}_j) (\mathbf{v}_i \cdot \mathbf{e}_k) \quad (15)$$

The last expression is obtained by computing the nonlinear fluxes inside the subspace and project those back to the full N -dimensional space.

The QG-DO UQ method provides dramatic improvement compared with the standard Galerkin order-reduction methods [15]. However, in systems with large number of instabilities, if s is not large enough to capture the complete nonlinear energy fluxes, the QG-DO scheme will not be able to equilibrate to the correct amount of energy leading to i) either severe underestimation of energy to sufficiently low levels where the modeled part of the fluxes can balance the corresponding (for this

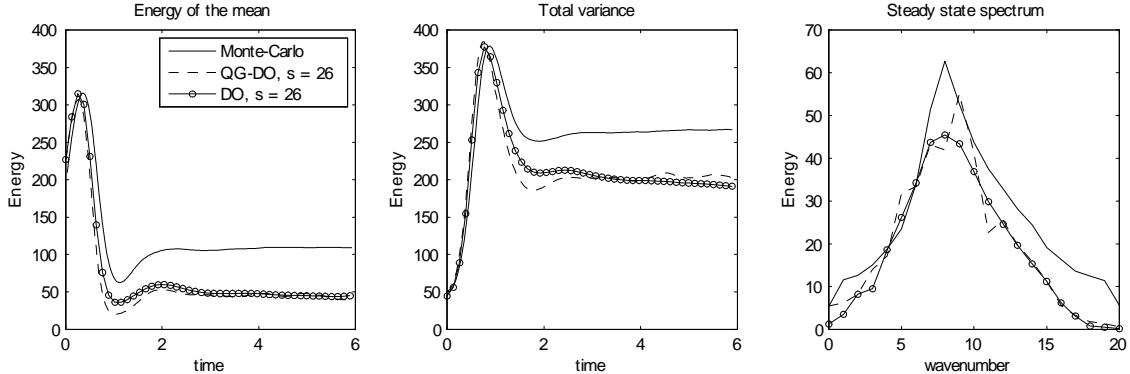


Figure 3: Misleading performance of QG-DO and DO method for the Lorenz 96 system with $F = 8$. In both cases a large number of modes is employed ($s = 26$).

energy level) number of instabilities, or ii) to blowup of the solution due to instabilities which are not balanced by negative nonlinear fluxes. The above two scenarios have been analyzed previously in the context of completely absent modeling of the nonlinear fluxes $Q_F = 0$ (quasilinear Gaussian closure) [16].

In Figure 5 (upper plots) we compare the performance of the QG-DO algorithm (using $s = 2$) with direct Monte-Carlo simulation in the unstable triad system presented in the previous section. As we described previously, the two low-energy modes act as energy channels and therefore by ignoring one of them we do not allow the UQ scheme to reach a statistical equilibrium creating important discrepancies both to the mean and the variance.

For L-96 the problems are even more important since in this case we know a priori (using the results of Fig. 2) that for $s \leq 14$ the captured portion of the nonlinear fluxes is close to zero and thus the QG-DO scheme behaves essentially like the QG closure with poor behavior documented and explained in [16]. To this end we increase the number of modes to $s = 26$ corresponding (according to Fig. 2) to a captured portion of the nonlinear fluxes greater than 50% and to a captured portion of total energy by the subspace that is greater than 80% (for $F = 8$). The results are presented in Fig. 3 for constant forcing in space and time: $F = 8$. We observe that there is an important underestimation of the energy of the mean - a feature caused by the misleading modeling of the nonlinear fluxes that cannot balance the number of instabilities occurring at the correct energy level. We also observe that there is essentially zero improvement compared with the DO method since the main cause of the failure is not misleading modeling of linear processes but rather insufficient modeling of the nonlinear mechanisms.

3.2 Modified quasi-linear Gaussian (MQG) method

In the MQG closure the modeling of the nonlinear fluxes is done by using statistical steady state information for a given set of forcing and system parameters [16]. In particular we consider the first two moment equations (2) and (4) associated with the original system with respect to an orthogonal, fixed basis \mathbf{v}_i . In the statistical steady state the nonlinear fluxes Q_F will satisfy the relation

$$L_v(\bar{\mathbf{u}}_\infty) R_\infty + R_\infty L_v^*(\bar{\mathbf{u}}_\infty) + Q_\sigma + Q_{F\infty} = 0.$$

We split the empirical fluxes into a positive semi-definite part $Q_{F\infty}^+$ and a negative semi-definite part $Q_{F\infty}^-$:

$$Q_{F\infty} = Q_{F\infty}^- + Q_{F\infty}^+.$$

Note that the empirical fluxes must satisfy **for every time instant** the conservative property of B which in the above context is expressed by the constraint:

$$Tr [Q_F] = 0 \Rightarrow Tr [Q_F^+] = -Tr [Q_F^-]. \quad (16)$$

The positive fluxes Q_F^+ indicate the energy being ‘fed’ on the stable modes in the form of external stochastic noise. On the other hand the negative fluxes Q_F^- should act directly on the positive part of the L_v -spectrum, effectively stabilizing the unstable modes. To achieve this we choose to represent the negative fluxes as additional damping

$$Q_F^-(R) = N_\infty R + RN_\infty^*$$

with N_∞ determined by solving the equation

$$Q_{F\infty}^- = N_\infty R_\infty + R_\infty N_\infty^*$$

which has a unique solution

$$N_\infty = \frac{1}{2} Q_{F\infty}^- R_\infty^{-1}.$$

In addition, as explained in detail in [16] we add a small amount of damping and noise to improve the marginal stability which otherwise occurs in the steady state. Moreover, we scale the fluxes with a suitable functional (here we use the square-root of the total energy) in order to achieve the best possible accuracy in the timescales of the system and the transient response. This will give the final MQG closure scheme:

$$\frac{d\bar{\mathbf{u}}}{dt} = [L + D] \bar{\mathbf{u}} + B(\bar{\mathbf{u}}, \bar{\mathbf{u}}) + R_{ij} B(\mathbf{v}_i, \mathbf{v}_j) + \mathbf{F} \quad (17a)$$

$$\frac{dR}{dt} = L_v R + RL_v^* + NR + RN^* + Q_F^+ + Q_\sigma \quad (17b)$$

$$N = \frac{1}{2} \frac{f(R)}{f(R_\infty)} (Q_{F\infty}^- - qI) R_\infty^{-1} \quad \text{and} \quad Q_F^+ = -\frac{Tr [Q_F^-]}{Tr [Q_{F\infty}^+]} (Q_{F\infty}^+ + qI) \quad (17c)$$

with $q = q_s \lambda_{\max} [Q_{F\infty}]$ and $f(R) = \sqrt{Tr(R)}$. The last formulation guarantees the conservation property (16) on every time-instant.

In the MQG closure the modeling of the nonlinear fluxes occurs in the second-order level and therefore no statistical information for higher order moments is required to be computed or measured. Essentially, we are using the steady information to determine the magnitude (for each degree of freedom) of the minimum amount of additional damping and additional noise required to approximate the effect of the nonlinear energy transfer terms. This additional damping will balance the linear, persistent instabilities while the additional noise will ‘feed’ the stable modes with energy.

The MQG closure presents remarkable performance even under forcing conditions that ‘push’ the system to energetic regimes which are very far from the tuning regime [16]. However, for forcing conditions which are strongly inhomogeneous in space and create local, in space, instabilities the additional damping and noise N, Q_F^+ (which have been computed for homogeneous conditions) may

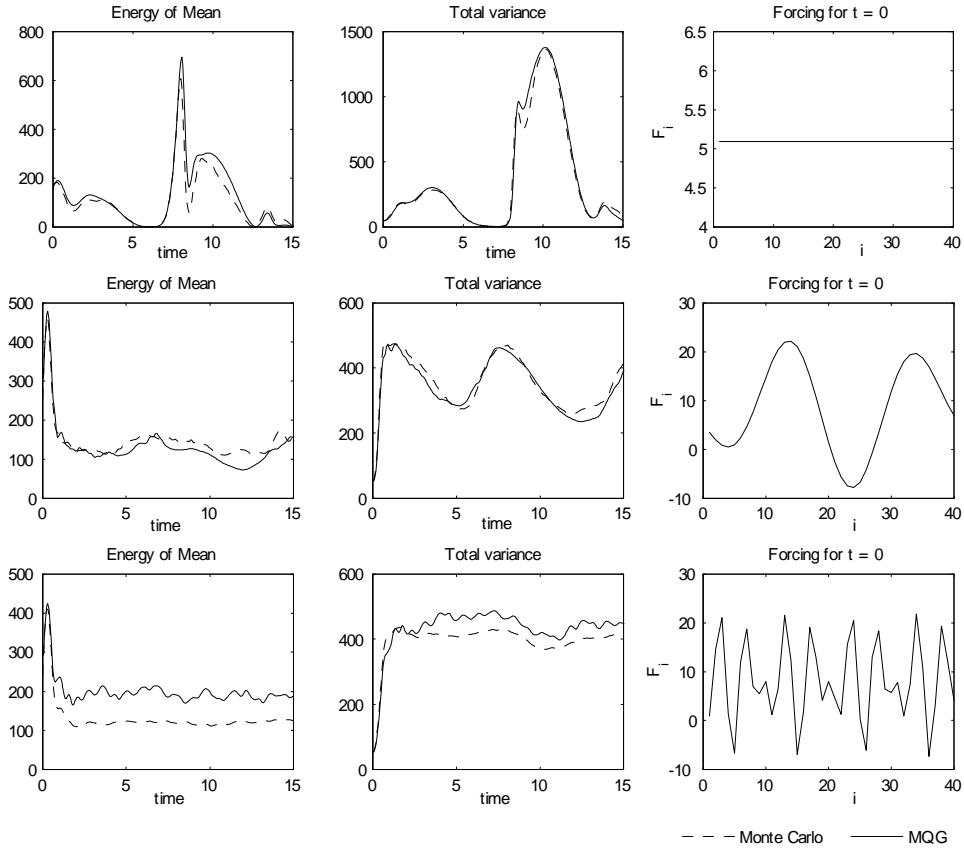


Figure 4: Comparison of MQG UQ scheme (solid line) with Monte-Carlo (dashed line) in L-96 for different spatial dependence of the forcing $F_i(t)$ (eq. (18)). First row: $a = 0$ - no spatial dependence; second row: $a = 0.2$ - weak spatial dependence; third row: $a = 1$ - strong spatial dependence. The tuning of the fluxes has been made using steady state statistics that correspond to constant forcing $F = 8$.

fail to capture the correct energy transfers. Here we measure the performance of the MQG closure scheme through the L-96 system with a strongly time-space dependent forcing given by

$$F_i(t) = F + 2F \sin\left(a\frac{3i}{10} - \frac{3t}{20}\right) \sin\left(a\frac{3i}{2} + \frac{3t}{4} + \pi\right), \quad 0 \leq i \leq 39 \quad (18)$$

where $F = 8$ and the nonlinear fluxes have been tuned based on the $F = 8$ steady state. Note that there are large inhomogeneous changes in the forcing magnitude compared to the tuning value for any a . In Figure 4 we observe that for $a = 0$ and $a = 0.2$, i.e. zero or slow spatial variation of the forcing but large changes in magnitude, the MQG algorithm has very good performance on capturing first and second order-moments. For much faster spatial variation of the forcing ($a = 1$) MQG is unable to adequately model the energy transfers. Therefore, despite its very good performance for homogeneous or close to homogeneous conditions, MQG may have important discrepancies in the case of strongly inhomogeneous excitations (Figure 4). Modeling such inhomogeneous responses will be the goal of the next section where the nonlinear fluxes will be modeled by combining ideas from reduced-order subspaces with the MQG approach.

4 A blended approach based on MQG and subspace generated nonlinear fluxes (MQG-DO method)

We saw that MQG has the most robust behavior in UQ of turbulent systems, compared with all the other UQ methodologies. However, for strong forcing or variation of system parameters additional instabilities may be introduced which cannot be modeled appropriately by the MQG fluxes. For this case we introduce a blended approach where the MQG fluxes will be improved through a reduced-subspace model which will run over a DO basis. The reduced order model that runs inside the subspace has also to take into account the energy fluxes coming from the nonlinear processes outside the subspace. To this end, we will have a two-way coupling between MQG and DO where i) the nonlinear fluxes of the MQG model will be corrected using higher-order stochastic information from the subspace, while ii) the evolution of the dynamics inside the subspace will take into account the nonlinear fluxes occurring due to the nonlinear interactions between the subspace modes and the orthogonal (to the subspace) modes, a feature that is captured by the MQG fluxes.

We will use a double representation for the solution. Similarly with the QG-DO method, we will represent the solution i) using a fixed, high-dimensional basis

$$\mathbf{u}_{MQG}(t) = \bar{\mathbf{u}}(t) + \sum_{i=1}^N Z_i(t; \omega) \mathbf{v}_i$$

and ii) a time-dependent, low dimensional basis

$$\mathbf{u}_{DO}(t) = \bar{\mathbf{u}}(t) + \sum_{i=1}^s Y_i(t; \omega) \mathbf{e}_i(t)$$

that represent the dynamics within a reduced-order subspace $\mathbf{V}_S = \text{span}[\mathbf{e}_i(t)]$. We require the two solutions to have the same mean and also to be identical inside the subspace. This is expressed by the condition

$$\mathbf{u}_{DO}(t) \cdot \mathbf{e}_i(t) = \mathbf{u}_{MQG}(t) \cdot \mathbf{e}_i(t), \quad \text{for } i = 1, \dots, s$$

or equivalently,

$$\sum_{j=1}^N Z_j \mathbf{v}_j \cdot \mathbf{e}_i = Y_i$$

which gives the *consistency condition* between the high dimensional covariance ($R = \langle \mathbf{Z}\mathbf{Z}^* \rangle$) and the reduced-order covariance ($C_{YY} = \langle \mathbf{Y}\mathbf{Y}^* \rangle$):

$$C_{YY} = P^* R P, \quad \text{where} \quad \mathbb{R}^{N \times s} \ni P_{ji} = \mathbf{v}_j \cdot \mathbf{e}_i \quad (19)$$

The MQG-DO UQ scheme is developed as follows.

- *Mean field equation*

The mean field equation that we will employ is that one that takes into account the high-dimensional covariance information - expressed through the covariance R . This is equation (2) rewritten here for convenience

$$\frac{d\bar{\mathbf{u}}}{dt} = [L + D] \bar{\mathbf{u}} + B(\bar{\mathbf{u}}, \bar{\mathbf{u}}) + R_{ij} B(\mathbf{v}_i, \mathbf{v}_j) + \mathbf{F}. \quad (20)$$

- *Evolution of the covariance matrix R*

We recall the second-order moment equation (eq. (4))

$$\frac{dR}{dt} = L_v R + R L_v^* + Q_F + Q_\sigma.$$

In the MQG approach we represent the nonlinear fluxes Q_F , using steady state information, through a positive definite (external noise) and negative definite (minimum additional dissipation) part. In the QG-DO this is done using higher-order statistical information inside the subspace. In this blended MQG-DO approach we will combine these ideas by using MQG fluxes but improving those (since they rely on steady state information) by correcting them using higher-order statistical information from the low dimensional subspace \mathbf{V}_S . In particular from the MQG nonlinear fluxes we will i) *subtract the steady state nonlinear fluxes* $Q_{V_S, \infty}$ that correspond to the subspace \mathbf{V}_S , and ii) we will add the corresponding fluxes computed using the high-order statistics of the subspace which also include transient dynamics information:

$$Q_F = Q_{MQG} + Q_{V_S} - Q_{V_S, \infty}. \quad (21)$$

where $Q_{MQG} = NR + RN^* + Q_F^+$ (see eq. (17c)). This correction of the nonlinear fluxes (i.e. Q_{V_S} instead of $Q_{V_S, \infty}$) will be able to take into account important transient, and spatially non-homogeneous effects. To this end the evolution equation for the full covariance will take the form

$$\frac{dR}{dt} = L_v R + R L_v^* + Q_\sigma + Q_{V_S} + Q_{MQG} - Q_{V_S, \infty}. \quad (22)$$

The next step is to write down explicit formulas for the fluxes Q_{V_S} and $Q_{V_S, \infty}$. The energy flux in the reduced order subspace will be given by

$$Q_{V_S} = \langle Y_m Y_n Y_k \rangle [(B(\mathbf{e}_m, \mathbf{e}_n) \cdot \mathbf{v}_i)(\mathbf{v}_j \cdot \mathbf{e}_k) + (B(\mathbf{e}_m, \mathbf{e}_n) \cdot \mathbf{v}_j)(\mathbf{v}_i \cdot \mathbf{e}_k)]$$

This is the nonlinear flux matrix inside the subspace projected back to the high dimensional basis. The above fluxes also sum up to zero since $V_S \subset \text{span}_i [\mathbf{v}_i]$ and therefore $\mathbf{e}_m = (\mathbf{v}_q \cdot \mathbf{e}_m) \mathbf{v}_q$. Thus we will have

$$\begin{aligned} \text{Tr} [Q_{V_S}] &= 2 \langle Y_m Y_n Y_k \rangle (B(\mathbf{e}_m, \mathbf{e}_n) \cdot \mathbf{v}_p) (\mathbf{v}_p \cdot \mathbf{e}_k) \\ &= 2 \langle Y_m Y_n Y_k \rangle (B(\mathbf{e}_m, \mathbf{e}_n) \cdot \mathbf{e}_k) = 0. \end{aligned}$$

To represent the steady state nonlinear fluxes within the subspace we use the steady state skewness (assumed to be known) suitably rescaled with the current variance of the system:

$$Q_{V_S, \infty} = \mu_{mnk, \infty} \sqrt{\langle Y_m^2 \rangle \langle Y_n^2 \rangle \langle Y_k^2 \rangle} [(B(\mathbf{e}_m, \mathbf{e}_n) \cdot \mathbf{v}_i) (\mathbf{v}_j \cdot \mathbf{e}_k) + (B(\mathbf{e}_m, \mathbf{e}_n) \cdot \mathbf{v}_j) (\mathbf{v}_i \cdot \mathbf{e}_k)]$$

where the steady state skewness coefficients are given by

$$\mu_{mnk, \infty} = \frac{\langle Y_{m, \infty} Y_{n, \infty} Y_{k, \infty} \rangle}{\sqrt{\langle Y_{m, \infty}^2 \rangle \langle Y_{n, \infty}^2 \rangle \langle Y_{k, \infty}^2 \rangle}}, \quad \text{with } Y_{m, \infty} = (\mathbf{u}_\infty - \bar{\mathbf{u}}_\infty) \cdot \mathbf{e}_m(t).$$

We emphasize that the time-dependence in the skewness coefficients $\mu_{mnk, \infty}$ comes only through the time-dependent modes. Additionally, we have by construction

$$\text{Tr} [Q_{MQG}] = \text{Tr} [Q_{V_S}] = \text{Tr} [Q_{V_S, \infty}] = 0.$$

Therefore, the nonlinear flux formulation (21) is consistent with the energy conservation property of the nonlinear operator B . Equation (22) expresses the first level of coupling, i.e. the influence of the DO subspace dynamics on the evolution of the high-dimensional covariance.

- *Evolution of the DO stochastic subspace*

The evolution of the DO basis will be done using the standard DO equations for the basis [14]

$$\begin{aligned} \frac{\partial \mathbf{e}_i}{\partial t} &= [L + D] \mathbf{e}_i + B(\bar{\mathbf{u}}, \mathbf{e}_i) + B(\mathbf{e}_i, \bar{\mathbf{u}}) + B(\mathbf{e}_m, \mathbf{e}_n) \langle Y_k Y_m Y_n \rangle C_{ik}^{-1} \\ &\quad - \mathbf{e}_j ([L + D] \mathbf{e}_i + B(\bar{\mathbf{u}}, \mathbf{e}_i) + B(\mathbf{e}_i, \bar{\mathbf{u}}) + B(\mathbf{e}_m, \mathbf{e}_n) \langle Y_k Y_m Y_n \rangle C_{ik}^{-1}) \cdot \mathbf{e}_j \end{aligned} \quad (23)$$

- *Reduced-order stochastic dynamics*

The last step of our scheme is the formulation of a reduced order dynamical system inside the time-dependent subspace. This will be formulated by minimally modifying the standard reduced-order model (obtained by Galerkin projection to the DO basis, i.e. eq. (13)) so that the subspace covariance (expressed through the coefficients \mathbf{Y}) is energetically consistent with the covariance of the coefficients \mathbf{Z} (consistency condition (19)). Differentiating equation (19) gives

$$\frac{dC_{YY}}{dt} = P^* \frac{dR}{dt} P + \dot{P}^* R P + P^* R \dot{P} \quad (24)$$

(where $\frac{dR}{dt}$ is known, given by equation (22)). This is the consistency constraint expressed in differential form.

On the other hand for the evolution of the dynamics inside the subspace we consider the standard Galerkin projection model with an additional damping matrix $N_C \in \mathbb{R}^{s \times s}$ and noise term $Q_C^{1/2} \in \mathbb{R}^{s \times s}$ that will represent the nonlinear interactions between modes of the subspace and the modes outside of it. With this ansatz we will have the reduced-order dynamical system

$$\frac{dY_i}{dt} = ((P^* L_v P)_{im} + N_{C,im}) Y_m + (Y_m Y_n - C_{YY,mn}) B(\mathbf{e}_m, \mathbf{e}_n) \cdot \mathbf{e}_i + \dot{W}_m Q_{C,im}^{1/2} + \dot{W}_k \sigma_k \cdot \mathbf{e}_i \quad (25)$$

In the above equation all the quantities are known except for the pair N_C and Q_C . This will be determined by using the differential constraint (24). In particular we formulate the second order equation for the covariance C_{YY} by using eq. (25)

$$\frac{dC_{YY}}{dt} = (P^* L_v P + N_C) C_{YY} + C_{YY} (P^* L_v P + N_C)^* + Q_C + P^* Q_\sigma P + P^* Q_{V_S} P \quad (26)$$

From the covariance consistency condition (eqs. (19), (24)) and the evolution equation for R (eq. (22)) we have

$$\frac{dC_{YY}}{dt} = P^* (L_v R + R L_v^* + Q_\sigma + Q_{V_S} + Q_{MQG} - Q_{V_S, \infty}) P + \dot{P}^* R P + P^* R \dot{P}$$

By equating the two right hand sides of the last two equations we obtain (also taking into account that $C_{YY} = P^* R P$)

$$\begin{aligned} N_C (P^* R P) + (P^* R P) N_C^* + Q_C \\ = P^* L_v [I - P P^*] R P + P^* R [I - P P^*] L_v^* P + P^* Q_{MQG} P - P^* Q_{V_S, \infty} P + \dot{P}^* R P + P^* R \dot{P} \end{aligned} \quad (27)$$

We recall that $Q_{MQG} = N R + R N^* + Q_F^+$ and we choose the positive definite matrix Q_C as follows

$$Q_C = P^* Q_F^+ P \quad (28)$$

which is always possible since Q_F^+ is by construction positive definite. Then equation (27) takes the form

$$\begin{aligned} N_C (P^* R P) + (P^* R P) N_C^* \\ = P^* (L_v [I - P P^*] + N) R P + P^* R ([I - P P^*] + N^*) L_v^* P - P^* Q_{V_S, \infty} P + \dot{P}^* R P + P^* R \dot{P} \end{aligned}$$

From which we obtain N_C

$$N_C = \frac{1}{2} \left[P^* ((L_v [I - P P^*] + N) R + R ([I - P P^*] L_v^* + N^*) - Q_{V_S, \infty}) P + \dot{P}^* R P + P^* R \dot{P} \right] (P^* R P)^{-1} \quad (29)$$

With the above construction it is guaranteed that the dynamics inside the subspace will always contain the correct second-order information (correct energy) by taking into account the nonlinear energy fluxes due to the nonlinear interactions with the dynamics outside the subspace. The above construction can also be seen as a generalized Galerkin projection that takes into account available information for the dynamics which are not spanned by the employed basis. *Equations (28) and (29) express the second level of coupling between MQG and DO, i.e. the influence of the MQG fluxes on the reduced-order dynamics.* This completes the set of equations for the MQG-DO UQ scheme.

Note that for $s = 0$, MQG-DO is simplified to the standard MQG scheme while for $s = N$ we recover the original equation. For $s = 1$ the dynamics in the DO subspace become linear since $B(\mathbf{e}_1, \mathbf{e}_1) \cdot \mathbf{e}_1 = 0$. Therefore we expect Gaussian statistics for the stochastic coefficient Y_1 . In this case the nonlinear fluxes Q_{V_S} generated by the subspace will vanish since $\langle Y_1^3 \rangle = 0$. On the other hand, the steady state fluxes $Q_{V_S, \infty}$ that we subtract will be non-zero since $\mu_{111, \infty}$ is based on exact statistics. Thus, for $s = 1$ we expect inferior performance compared with MQG.

4.1 Consistency of the MQG-DO with the exact steady state statistics

Here we will prove that the MQG-DO UQ method will result in the correct steady state statistics. Essentially, we will need to prove that the steady state of the MQG-DO scheme is compatible with the exact steady state statistics. First we observe that

$$\begin{aligned} Q_{V_S} |_{\mathbf{Y}_\infty} &= \langle Y_{m\infty} Y_{n\infty} Y_{k\infty} \rangle [(B(\mathbf{e}_m, \mathbf{e}_n) \cdot \mathbf{v}_i)(\mathbf{v}_j \cdot \mathbf{e}_k) + (B(\mathbf{e}_m, \mathbf{e}_n) \cdot \mathbf{v}_j)(\mathbf{v}_i \cdot \mathbf{e}_k)] \\ &= \mu_{mnk, \infty} \sqrt{\langle Y_{m\infty}^2 \rangle \langle Y_{n\infty}^2 \rangle \langle Y_{k\infty}^2 \rangle} [(B(\mathbf{e}_m, \mathbf{e}_n) \cdot \mathbf{v}_i)(\mathbf{v}_j \cdot \mathbf{e}_k) + (B(\mathbf{e}_m, \mathbf{e}_n) \cdot \mathbf{v}_j)(\mathbf{v}_i \cdot \mathbf{e}_k)] \\ &= Q_{V_S, \infty}. \end{aligned}$$

We will also have

$$\begin{aligned} \left. \frac{dR}{dt} \right|_{\bar{\mathbf{u}}_\infty, R_\infty, \mathbf{Y}_\infty} &= L_v(\bar{\mathbf{u}}_\infty) R_\infty + R_\infty L_v^*(\bar{\mathbf{u}}_\infty) - \lim_{t \rightarrow \infty} Q_{V_S} + Q_{MQG} + Q_{V_S, \infty} + Q_\sigma \\ &= L_v(\bar{\mathbf{u}}_\infty) R_\infty + R_\infty L_v^*(\bar{\mathbf{u}}_\infty) + Q_{MQG} + Q_\sigma = 0 \end{aligned}$$

where the last equation vanishes by the construction of the MQG nonlinear fluxes Q_{MQG} .

Next, we consider the equation for the coefficients (25). By construction the covariance of the coefficients satisfies equation (24). Therefore, assuming that the subspace has converged to a steady state, i.e. $\dot{P} = 0$ we obtain that for $\mathbf{Y} = \mathbf{Y}_\infty$, $\bar{\mathbf{u}} = \bar{\mathbf{u}}_\infty$, $R = R_\infty$

$$\left. \frac{dC_{YY}}{dt} \right|_{\bar{\mathbf{u}}_\infty, R_\infty, \mathbf{Y}_\infty} = 0.$$

The mean equation is trivially satisfied. Thus, the MQG-DO model is indeed consistent (up to second order), by construction, with the correct steady state information.

4.2 Summary of the MQG-DO equations

Here we present a summary of the blended MQG-DO method for the convenience of the reader.

Equation for mean and covariance

$$\begin{aligned} \frac{d\bar{\mathbf{u}}}{dt} &= [L + D] \bar{\mathbf{u}} + B(\bar{\mathbf{u}}, \bar{\mathbf{u}}) + R_{ij} B(\mathbf{v}_i, \mathbf{v}_j) + \mathbf{F}, \\ \frac{dR}{dt} &= L_v R + R L_v^* + Q_\sigma + Q_{V_S} + Q_{MQG} - Q_{V_S, \infty}. \end{aligned} \tag{30}$$

where,

$$\begin{aligned}
Q_{MQG} &= NR + RN^* + Q_F^+ \\
N &= \frac{1}{2} \frac{f(R)}{f(R_\infty)} (Q_{F\infty}^- - qI) R_\infty^{-1} \quad \text{and} \quad Q_F^+ = -\frac{\text{Tr}[Q_F^-]}{\text{Tr}[Q_{F\infty}^+]} (Q_{F\infty}^+ + qI) \\
Q_{F\infty}^- + Q_{F\infty}^+ &= Q_{F\infty} = -L_v(\bar{\mathbf{u}}_\infty) R_\infty - R_\infty L_v^*(\bar{\mathbf{u}}_\infty) - Q_\sigma \\
q &= q_s \lambda_{\max}[Q_{F\infty}] \quad \text{and} \quad f(R) = \sqrt{\text{Tr}(R)},
\end{aligned}$$

and

$$\begin{aligned}
Q_{V_S} &= \langle Y_m Y_n Y_k \rangle [(B(\mathbf{e}_m, \mathbf{e}_n) \cdot \mathbf{v}_i)(\mathbf{v}_j \cdot \mathbf{e}_k) + (B(\mathbf{e}_m, \mathbf{e}_n) \cdot \mathbf{v}_j)(\mathbf{v}_i \cdot \mathbf{e}_k)] \\
Q_{V_{S,\infty}} &= \langle Y_{m\infty} Y_{n\infty} Y_{k\infty} \rangle [(B(\mathbf{e}_m, \mathbf{e}_n) \cdot \mathbf{v}_i)(\mathbf{v}_j \cdot \mathbf{e}_k) + (B(\mathbf{e}_m, \mathbf{e}_n) \cdot \mathbf{v}_j)(\mathbf{v}_i \cdot \mathbf{e}_k)].
\end{aligned}$$

Equation for the subspace basis

$$\begin{aligned}
\frac{\partial \mathbf{e}_i}{\partial t} &= [L + D] \mathbf{e}_i + B(\bar{\mathbf{u}}, \mathbf{e}_i) + B(\mathbf{e}_i, \bar{\mathbf{u}}) + B(\mathbf{e}_m, \mathbf{e}_n) \langle Y_k Y_m Y_n \rangle C_{ik}^{-1} \\
&\quad - \mathbf{e}_j ([L + D] \mathbf{e}_i + B(\bar{\mathbf{u}}, \mathbf{e}_i) + B(\mathbf{e}_i, \bar{\mathbf{u}}) + B(\mathbf{e}_m, \mathbf{e}_n) \langle Y_k Y_m Y_n \rangle C_{ik}^{-1}) \cdot \mathbf{e}_j.
\end{aligned} \tag{31}$$

Equation for the subspace dynamics

$$\frac{dY_i}{dt} = ((P^* L_v P)_{im} + N_{C,im}) Y_m + (Y_m Y_n - C_{Y, mn}) B(\mathbf{e}_m, \mathbf{e}_n) \cdot \mathbf{e}_i + \dot{W}_m Q_{C,im}^{1/2} + \dot{W}_k \sigma_k \cdot \mathbf{e}_i, \tag{32}$$

where $P_{ij} = \mathbf{v}_i \cdot \mathbf{e}_j$ and

$$\begin{aligned}
N_C &= \frac{1}{2} \left[P^* ((L_v [I - PP^*] + N) R + R ([I - PP^*] L_v^* + N^*) - Q_{V_{S,\infty}}) P + \dot{P}^* R P + P^* R \dot{P} \right] (P^* R P)^{-1} \\
Q_C &= P^* Q_F^+ P.
\end{aligned}$$

4.2.1 Numerical implementation of the MQG-DO scheme

The numerical implementation of the MQG-DO scheme is as follows:

- i) Computation of the current third-order statistics inside the subspace and subsequent computation of the subspace nonlinear fluxes Q_{V_S} , $Q_{V_{S,\infty}}$ (s -dimensional computation).
- ii) Evolution of the DO modes with a first-order Euler method (s -dimensional computation).
- iii) With fixed nonlinear fluxes from step i) we evolve the nonlinear equations (30) for a numerical time step using a 4th order Runge-Kutta method (N -dimensional computation).
- iii) We compute the matrices N_C and Q_C using the evolved values of R and $\bar{\mathbf{u}}$ from the previous step (s -dimensional computation).
- iv) We evolve the stochastic coefficients Y_i for a numerical time step using a 4th order Runge-Kutta method on eq. (32) with fixed matrices N_C and Q_C given by the previous step (s -dimensional computation).
- v) We perform orthonormalization of the DO modes and the stochastic coefficients to avoid numerical errors according to the procedure described in [18] (Section 5.2) (s -dimensional computation).

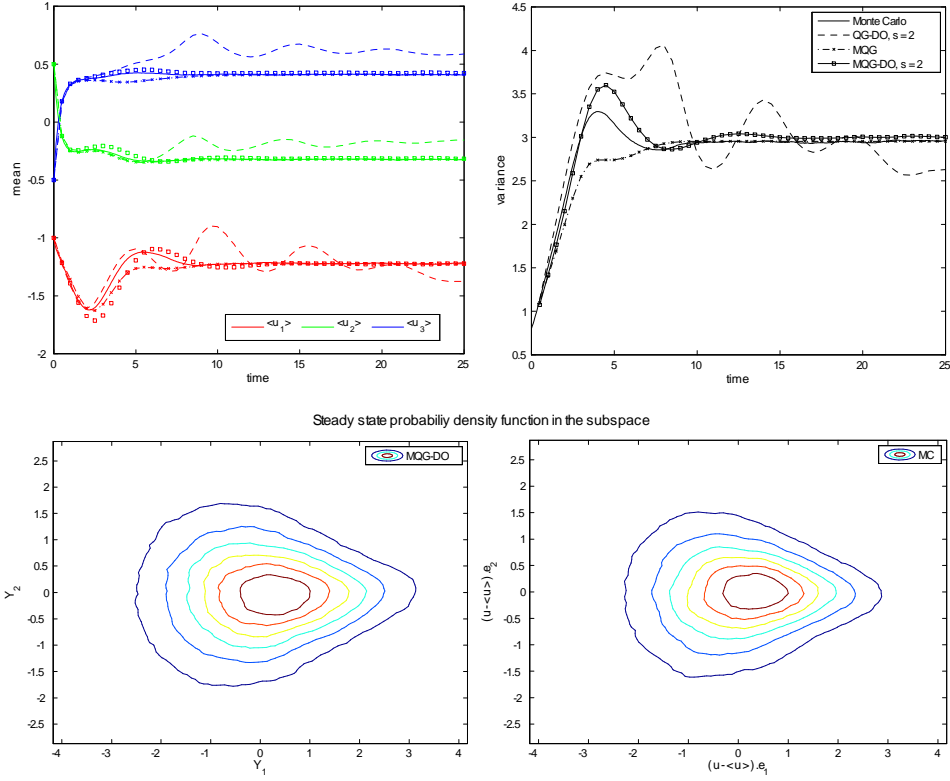


Figure 5: Triad system in an unstable configuration with constant forcing/parameters resolved with various UQ methods. The mean and the variance are plotted. In the lower plots a comparison is given between the pdf inside the subspace computed with *MQG – DO* and direct Monte-Carlo.

5 Application of MQG-DO to systems with unstable dynamics

Here we apply the new blended algorithm to the two unstable systems presented previously. We will consider for each system two configurations: i) a case with constant parameters where the system reaches the steady state which has been used to tune the MQG fluxes, and ii) a case where we have explicit time-dependence to the system/forcing parameters. This time dependence is chosen so that it ‘pushes’ the system away from the energetic regime for which the steady state statistics have been computed by introducing additional instabilities.

5.1 Triad system with unstable mean state

5.1.1 Steady state dynamics

The first case that we consider is the triad system in the unstable configuration presented in Section 2.1. In Figure 5 we compare the performance of the MQG-DO with direct Monte-Carlo simulation and with other UQ methods (MQG and QG-DO). Note that the performance of the QG-DO UQ scheme for the constant forcing case has been discussed already in Section 3.1 and it will not be considered here. For MQG we observe that even though it recovers very well the steady state performance it presents some discrepancies during the transient regime, especially in the variance. On the other hand MQG-DO with 2 modes is able to resolve much more effectively the transient dynamics while it still maintains the very good performance of MQG in the steady state. In addition, through MQG-DO we are able to recover the full non-Gaussian statistical steady state statistics inside the DO subspace which compare favorably with the exact ones (Fig. 5). This is due to the fact that the fluxes are partially resolved explicitly

5.1.2 Time dependent forcing

To illustrate more clearly the advantages of the MQG-DO method we consider a case where both the forcing and the system parameters fluctuate over time. Their fluctuations are chosen so that the system moves between dynamical regimes of zero, one, and two instabilities. Note that the steady state statistics are chosen based on the response of the previous (constant-parameters) configuration where only one instability is present. In particular the triad system that we consider has the form

$$\begin{aligned} du_1 &= (-\gamma_1 u_1 + \lambda_{12} u_2 + \lambda_{13} u_3 + \beta_1 u_3 u_2 + g_1) dt + (\sigma_1 + f^2 (\sigma_{T1} - \sigma_1)) dW_1 \\ du_2 &= (-\gamma_2 u_2 - \lambda_{12} u_1 + \lambda_{23} u_3 + \beta_2 u_1 u_3 + g_2) dt + (\sigma_2 + f^2 (\sigma_{T2} - \sigma_2)) dW_2 \\ du_3 &= (-\gamma_3 u_3 - \lambda_{13} u_1 - \lambda_{23} u_2 + \beta_3 u_2 u_1 + g_3) dt + (\sigma_3 + f^2 (\sigma_{T3} - \sigma_3)) dW_3 \end{aligned}$$

where the system parameters remain as in Section 2.1 and g_1, g_2, g_3 , and f are functions of time. Moreover, we choose the new additional parameters for the noise as $\sigma_{Ti} = \frac{3}{5}\sigma_i$ so that important variations in the noise intensity occur. We consider two cases for the time dependent functions: a time-periodic and one with random time dependence. For the periodic case we choose

$$g_1(t) = 0, \quad g_2(t) = -1 + 0.5 \sin \frac{\pi t}{2}, \quad g_3(t) = 1 + 0.2 \cos \frac{\pi t}{2}, \quad f(t) = 1.3 \sin \frac{\pi t}{2}$$

and as we observe in Figure 6 (lower-left subplot) the system oscillates between a stable and an unstable regime with one instability. The blended MQG-DO method ($s = 2$) recovers very well both the periodic attractor and the initial transient regime in terms of the first and second order statistics. MQG does very well for the mean but it cannot track the second-order statistics very effectively. This is due to the fact that MQG has been tuned for a dynamical regime with one unstable direction and, as the results indicate, the correct nonlinear fluxes are not effectively represented in the fully stable regime. This is also the case for QG-DO where nonlinear fluxes are partially represented through the non-Gaussian statistics inside the DO subspace. By comparing QG-DO and MQG we can conclude that for unstable systems it is more effective to use a complete (full-order) model of the nonlinear fluxes based on steady state statistics which may refer to a different energy/dynamical regime rather than model the nonlinear fluxes using an explicit approach such as QG-DO which gives an incomplete (reduced-order) representation of the nonlinear dynamics and creates important discrepancies.

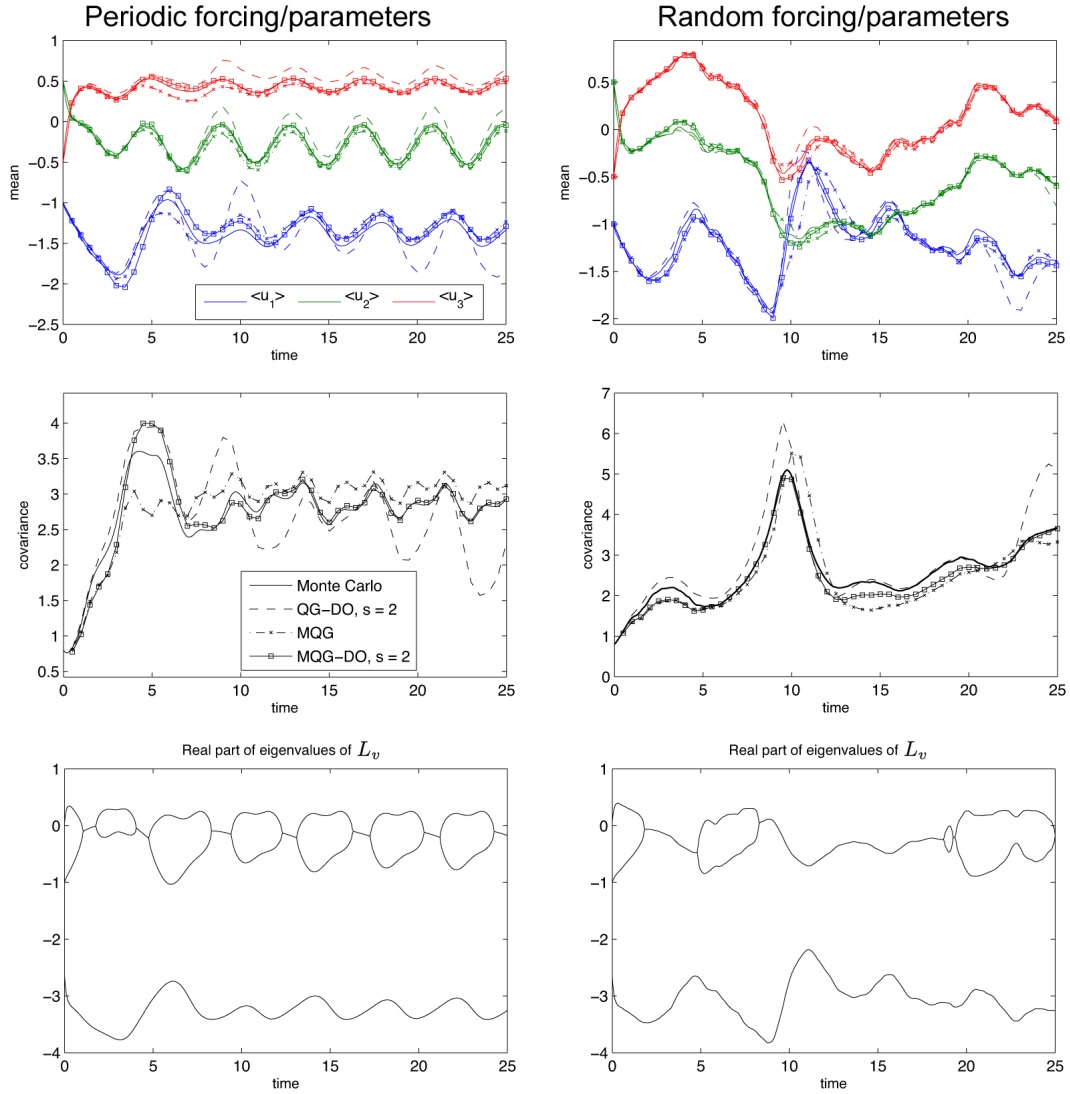


Figure 6: Triad system with time dependent parameters and forcing. The system oscillates between a stable and an unstable regime. The performance of MQG-DO algorithm is compared with Monte-Carlo and other UQ methods.

In the case with random time-dependence we have the functions g_i given by

$$\mathbf{g}(t) = \begin{pmatrix} 0 \\ -1 \\ 1 \end{pmatrix} + g(t) \begin{pmatrix} 1 \\ 1 \\ 1 \end{pmatrix} \quad \text{where} \quad dg = -\frac{1}{4}g + 0.4\sqrt{\frac{1}{2}}dW_g(t; \omega)$$

and the noise intensity is also controlled by an Ornstein–Uhlenbeck (OU) process

$$df = -\frac{1}{4}f + 0.7\sqrt{\frac{1}{2}}dW_f(t; \omega).$$

In Figure 6 (lower-right subplot) we show the resulted evolution of the eigenvalues for the linearized dynamics. The transition involves fully stable and unstable regimes with one and two instabilities. From Figure 6 (second plot on the right column) we observe the explosion of variance occurring right after the system passes very briefly through the regime with two instabilities ($t \sim 7.5$). MQG-DO ($s = 2$) is able to track very effectively this unstable transition while QG-DO and MQG overestimate the system variance since they cannot model the correct nonlinear fluxes during the subsequent stable phase. Similarly with the periodic case MQG performs very well for the estimation of the mean given its extremely inexpensive computational character. When we compare MQG with QG-DO we can make similar conclusions with the periodic case, i.e. that an empirical, but nevertheless complete (full-order) model, of the nonlinear fluxes (such as MQG) performs much better than a scheme that explicitly model the nonlinear fluxes through a reduced order approach.

5.2 Lorenz 96 with time-space dependent forcing

The second application where we illustrate and validate MQG-DO method is the Lorenz 96 system presented in Section 2.2. Similarly with the triad system we will consider two cases: i) constant parameters where a statistical steady state is reached, and ii) strongly time-space dependent forcing.

5.2.1 Steady-state dynamics

For this constant parameters case we choose $F = 8$ and we use the second order statistics describing the statistical steady state to obtain the MQG nonlinear fluxes. Then we resolve the transient problem in order to examine how well the blended MQG-DO method does on capturing the transient dynamics, the steady state spectrum, and also recovering the higher-order statistical structures inside the subspace. Based on the study of the nonlinear energy fluxes that we presented previously (Fig. 2), we obtain an estimate of the maximum improvement on the nonlinear fluxes, by resolving s modes within the DO subspace. For example we can immediately conclude that if $s < 15$ the impact of the DO correction to the MQG nonlinear fluxes will be less than 2-3%. To this end we choose $s = 26$ so that we have equal orders of contribution between the MQG and the DO component.

Note that due to the special geometry of the triad interactions occurring in the Lorenz 96 system the problem is particularly hard. In more realistic turbulent systems we do not expect the very low-energy modes to directly interact with the largest energy modes. In this case we rather expect strong triad interactions between high and intermediate energy modes and subsequent flow of energy through the inertial scales to the dissipations scales.

In Figure 7 we present the performance of the MQG-DO scheme with $s = 26$ modes. The recovery of the correct spectrum indicates that the two-level coupling between MQG and DO

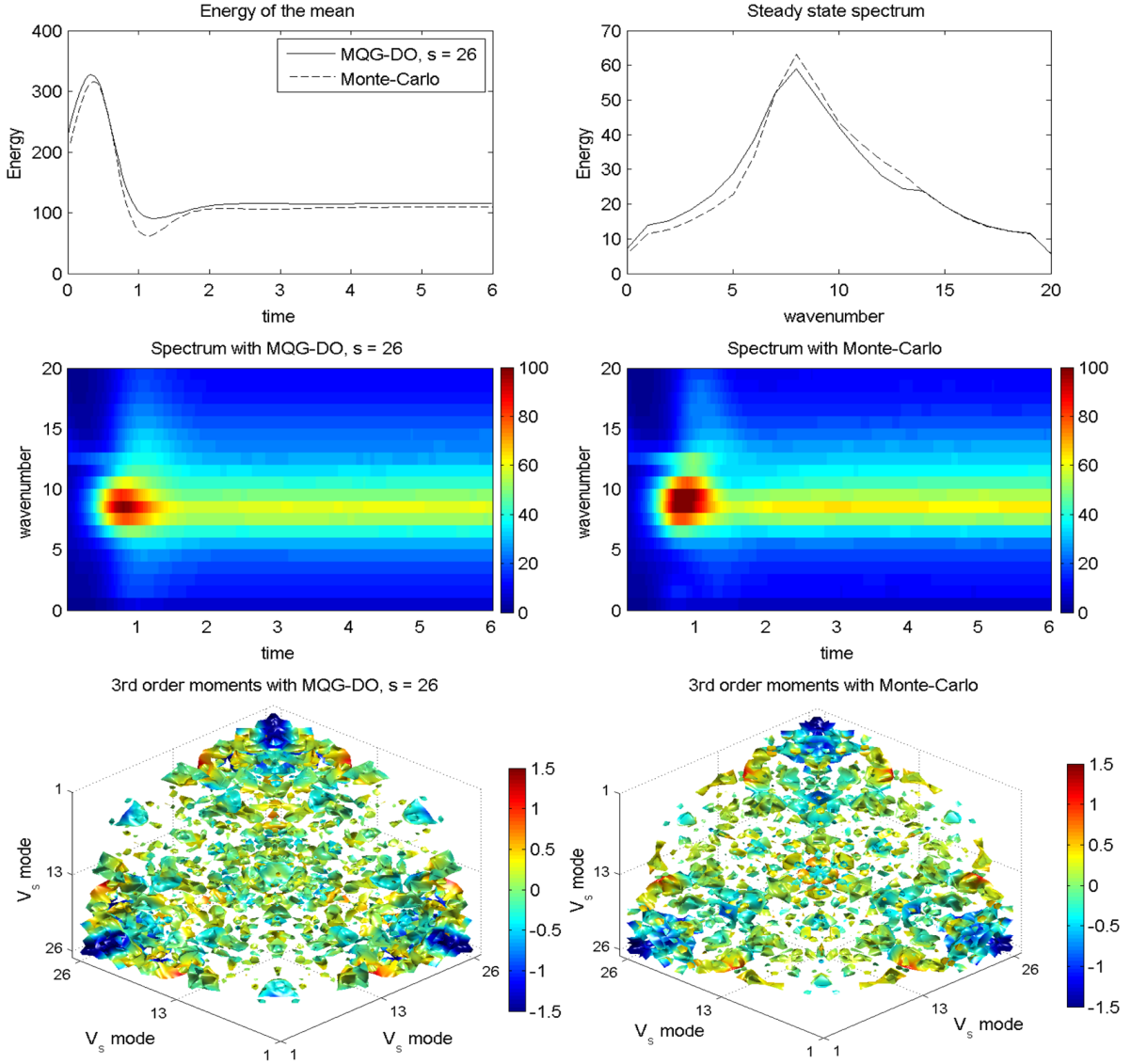


Figure 7: Lorenz-96 system for $F = 8$ resolved with MQG-DO method and $s = 26$. The time series for the mean, the spectrum, and the third-order central moments within the subspace are shown and compared with direct Monte-Carlo. The plotting of the third order moments follows the same technique used in Figure 2.

occurs naturally without causing important discrepancies. This is also suggested by the higher-order statistics in steady state. In particular in the lower plots of Figure 7 we present the third order moments in steady state $M_{ijk} = \langle Y_{\infty i} Y_{\infty j} Y_{\infty k} \rangle$ as those are computed with MQG-DO and with direct Monte-Carlo. In particular we plot only the moments that have values for which $|M_{ijk}| > 0.15 \max_{ijk} M_{ijk}$ and we color those according to their values. Through these results we can clearly see that the third order moments inside the subspace are recovered very effectively even though a full Monte-Carlo scheme is run only for the DO dynamics inside the subspace.

5.2.2 Time-space dependent forcing

Here we consider the strongly forced Lorenz 96 presented in Section 3.2 in the extreme regime where the MQG scheme fails to perform UQ adequately. In particular we consider the forcing given by equation (18) with $a = 1$. The spatiotemporal pattern of the excitation is shown in Figure 8 (upper-left subplot). Under the effect of this excitation we inject energy directly to the high wavenumber modes and an important portion of it is transferred back to the small-wavenumber modes. MQG is not capable to model adequately this energy transfer since it has been calibrated in a completely different dynamical regime where such energy transfers do not occur. To this end, as we can observe in the MQG spectrum of Figure 8, energy is overestimated in the high wavenumber modes while the low wavenumber modes have smaller energy than the Monte-Carlo simulation.

On the other hand, MQG-DO directly models an important part of the nonlinear energy fluxes. As we observe in Figure 9 the DO modes localize exactly in the locations where the high frequency forcing is active. The non-Gaussian statistics in the stochastic subspace explicitly model the nonlinear fluxes from the high wavenumber modes to the low-wavenumber modes. However, as explained previously, due to the peculiarity of the nonlinear interactions in Lorenz 96, we need an important number of modes in order to have an effective correction of the MQG nonlinear fluxes (which do not take into account the time-space character of the external excitation). Therefore for $s = 14$ the improvement is minimal and is restricted in the low-wavenumber modes of the spectrum. For a larger subspace ($s = 20$) things are improved more but still the large-wavenumber modes do not carry completely the correct amount of energy to the low-energy modes. This is achieved when $s = 26$ where the obtained spectrum has very good agreement with the exact spectrum. Note that some minor discrepancies are expected since still we do not resolve the full nonlinear energy fluxes and an important portion of them is based on steady state information.

In Figure 8 we also present the time series for the energy of the mean and the trace of the covariance. We can immediately conclude the monotonic convergence to the Monte-Carlo statistics as the number of modes is increasing. This is another manifestation of the natural coupling between the MQG and the DO components that results in pure improvement of the MQG. Finally, in Fig 10 we present the third order moments inside the subspace as those are computed for $t = 8$ using the MQG-DO scheme and a direct Monte-Carlo simulation. We emphasize that these results refer to a transient problem and even though the agreement is not in the point-wise sense we still have a very satisfactory estimation of the nonlinear interactions inside the subspace.

6 Conclusions and Future directions

We have presented a blending framework between inexpensive, full-space, second-order methods based on diagnostic nonlinear energy fluxes from a steady-state (MQG) and high-statistical-order

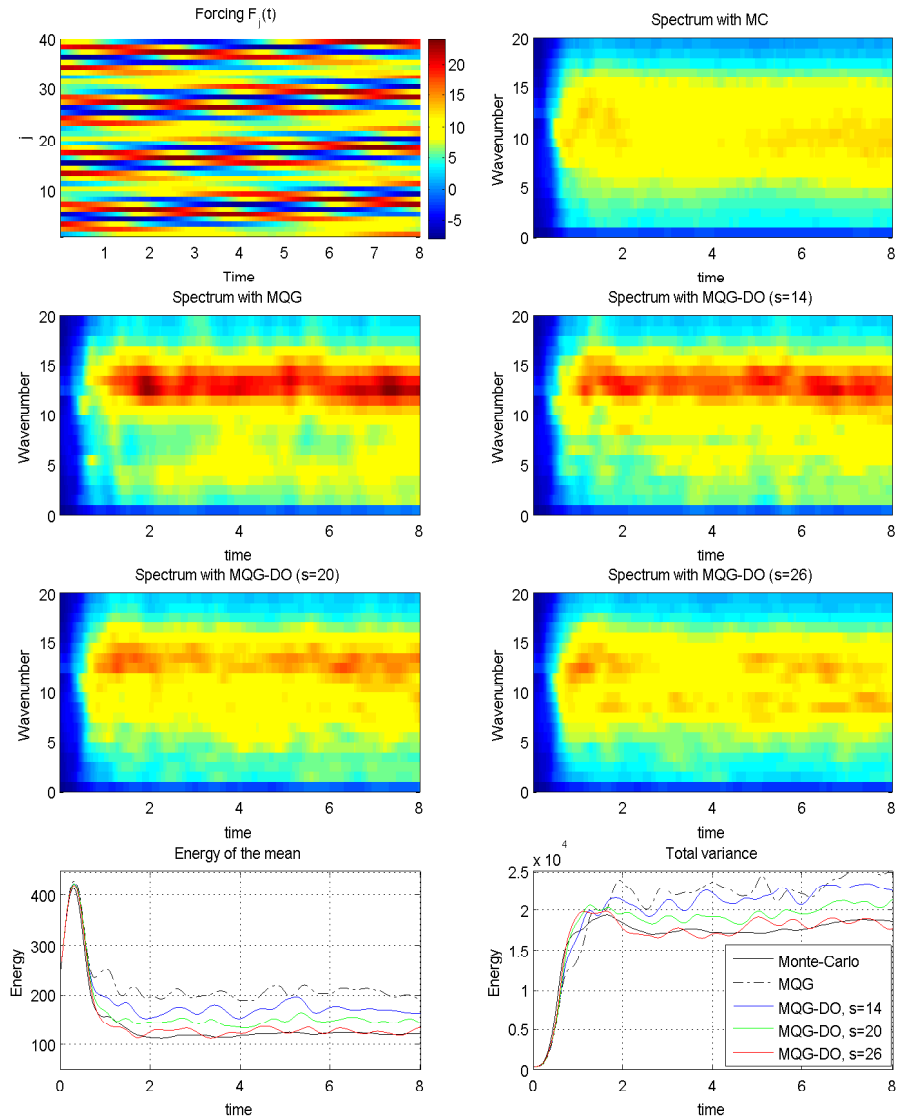


Figure 8: Lorenz 96 system with extreme time and space dependent forcing. The performance of MQG and MQG-DO methods (for various s) is shown and compared with Monte-Carlo in terms of the spectrum, the energy of the mean, and the total stochastic energy.

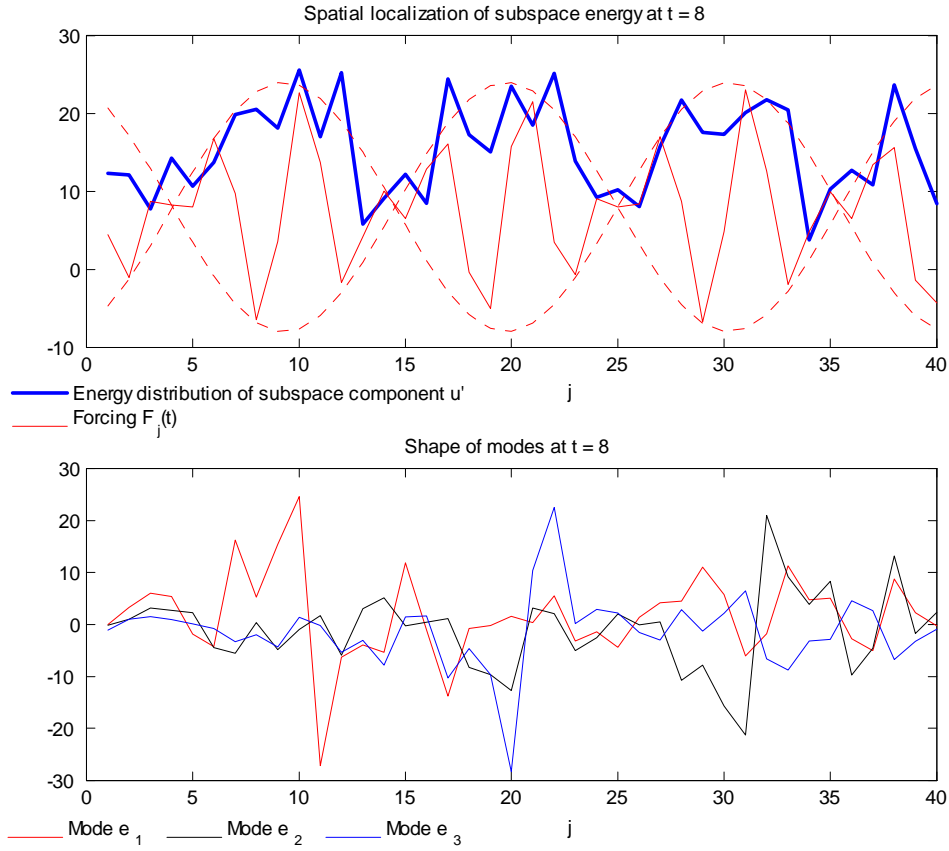


Figure 9: Upper plot: Localization of the energy spanned by the DO modes $\{\mathbf{e}_j\}_{j=1}^{26}$ expressed through the grid point energy density $\sum_{m,n=1}^{26} C_{YY,mn} e_{mk} e_{nk}$ for $t = 8$ and $s = 26$ (blue bold curve); the forcing $F_j(t)$ for $t = 8$ (red solid curve) plotted together with the large scale modulation envelope of the forcing. Lower plot: The first three modes \mathbf{e}_1 , \mathbf{e}_2 , \mathbf{e}_3 for $t = 8$.

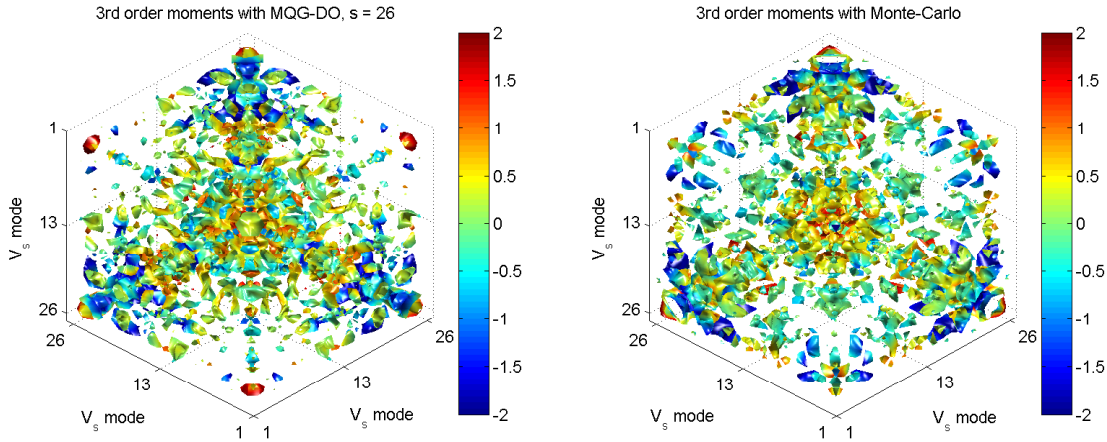


Figure 10: Comparison of third-order central-moments for Lorenz 96 subjected to extreme excitation. The moments inside the subspace are shown (for $t = 8$) computed with MQG-DO ($s = 26$) and Monte-Carlo. The visualization follows the same technique used in Figure 2.

methods for reduced-order subspaces (DO). The coupling of these two methodologies presents particular challenges due to the contradictory nature of the two ingredients. Based on energy fluxes arguments we establish a two-way coupling by i) correcting the MQG nonlinear energy fluxes using non-Gaussian statistical information from the DO subspace, and ii) correct the reduced order dynamics inside the subspace so that the interactions with dynamical components outside the subspace are fully taken into account.

With this blended MQG-DO method we prove that i) the steady state statistics are still recovered correctly (as it happens in the MQG method), and ii) we obtain a pure improvement compared with the MQG method, which increases monotonically as the number of modes, whose full statistics are modeled, increases. We illustrate the blended approach in two unstable systems (where MQG and order-reduction approaches fail to approximate correctly) under extreme excitation scenarios involving localized forcing and energy injected in high-wavenumber modes. The results indicate that the MQG-DO method is able to recover the correct evolution of the spectrum and the mean (second-order statistics) over the full dimensionality of the system, but also approximate satisfactorily the higher order statistics within the stochastic subspace. Future work includes the application of the above framework in realistic turbulent systems using a combination of DO and carefully chosen, fixed modes. Also, the above methodology has great potential for the correct quantification of non-Gaussian statistics and in particular extreme events for specific modes of interest (e.g. extreme waves in the ocean, etc.).

Acknowledgment. The research of A. Majda is partially supported by NSF grant DMS-0456713, NSF CMG grant DMS-1025468, and ONR grants ONR-DRI N00014-10-1-0554, N00014-11-1-0306 and ONR-MURI N00014-12-1-0912. T. Sapsis is supported as postdoctoral fellow on the first and third grants.

References

- [1] T. DelSole, *Stochastic models of quasigeostrophic turbulence*, *Surv. Geophys.*, 25 (2004), pp. 107–149.
- [2] P. Holmes, J. Lumley, and G. Berkooz, *Turbulence, Coherent Structures, Dynamical Systems and Symmetry*, Cambridge University Press, 1996.
- [3] S. Lall, J. E. Marsden, and S. Glavaski, *A subspace approach to balanced truncation for model reduction of nonlinear control systems*, *Int. J. Robust Nonlinear Control*, 12 (2002), p. 519.
- [4] E. Lorenz, *Predictability - a problem partly solved*, in *Proceedings on Predictability*, ECMWF, September 1996, pp. 1–18.
- [5] E. N. Lorenz and K. A. Emanuel, *Optimal sites for supplementary weather observations: Simulations with a small model*, *J. Atmos. Sci.*, 55 (1998), pp. 399–414.
- [6] Z. Ma, C. W. Rowley, and G. Tadmor, *Snapshot-based balanced truncation for linear time-periodic systems*, *IEEE Trans. Autom. Control*, 55 (2010), p. 469.
- [7] A. J. Majda, R. V. Abramov, and M. J. Grote, *Information Theory and Stochastics for Multi-scale Nonlinear Systems*, vol. 25 of CRM Monograph Series, American Mathematical Society, 2005.
- [8] A. J. Majda, B. Gershgorin, and Y. Yuan, *Low-frequency climate response and fluctuation-dissipation theorems: Theory and practice*, *J. Atmos. Sci.*, 67 (2010), pp. 1186–1201.
- [9] A. J. Majda and J. Harlim, *Filtering Complex Turbulent Systems*, Cambridge University Press, 2012.
- [10] A. J. Majda, I. Timofeyev, and E. Vanden-Eijnden, *Models for stochastic climate prediction*, *Proceedings of the National Academy of Sciences*, 96 (1999), p. 14687.
- [11] ———, *A mathematical framework for stochastic climate models*, *Comm. Pure Appl. Math.*, 54 (2001), p. 891.
- [12] ———, *A priori tests of a stochastic mode reduction strategy*, *Physica D*, 170 (2002), p. 206.
- [13] T. P. Sapsis, *Attractor dimensionality, nonlinear energy transfers, and finite-time instabilities in unstable dynamical systems with applications to 2D Navier-Stokes equations*, submitted, (2012).
- [14] T. P. Sapsis and P. F. J. Lermusiaux, *Dynamically orthogonal field equations for continuous stochastic dynamical systems*, *Physica D*, 238 (2009), pp. 2347–2360.
- [15] T. P. Sapsis and A. J. Majda, *Blended reduced subspace algorithms for uncertainty quantification of quadratic systems with a stable mean state*, *Physica D* (Submitted), (2012).
- [16] ———, *A statistically accurate modified quasilinear gaussian closure for uncertainty quantification in turbulent dynamical systems*, *Physica D* (Submitted), (2012).

- [17] L. Sirovich, *Turbulence and the dynamics of coherent structures, parts I, II and III*, Quart. Appl. Math., XLV (1987), pp. 561–590.
- [18] M. P. Ueckermann, P. F. J. Lermusiaux, and T. P. Sapsis, *Efficient numerical discretization of stochastic Navier-Stokes equations with the dynamical orthogonality condition and projection methods*, J. Comput. Phys., (2012).